The Re-Initiation of Cellular Detonations Downstream of an Inert Layer

Kelsey C. Tang-Yuk[a], John H.S. Lee[a], Hoi Dick Ng[b], Ralf Deiterding[c], XiaoCheng Mi[d,e,*]

[a] *McGill University, Montreal, QC, Canada.*
[b] *Concordia University, Montreal, QC, Canada.*
[c] *University of Southampton, Southampton, United Kingdom.*
[d] *Department of Mechanical Engineering, Eindhoven University of Technology, Eindhoven, the Netherlands.*
[e] *Eindhoven Institute of Renewable Energy Systems, Eindhoven University of Technology, Eindhoven, the Netherlands.*

Abstract

The current work aims to examine how the nature of cellular instabilities controls the re-initiation capability and dynamics of a gaseous detonation transmitting across a layer of inert (or non-detonable) gases. This canonical problem is tackled via computational analysis based on the two-dimensional, reactive Euler equations. Two different chemical kinetic models were used, a simplified two-step induction-reaction model and a detailed model for hydrogen-air. For the two-step model, cases with relatively high and low activation energies, representing highly and weakly unstable cellular detonations, respectively, are considered. For the weakly unstable case, two distinct types of re-initiation mechanisms were observed. (1) For thin inert layers, at the exit of the layer the detonation wave front has not fully decayed and thus the transverse waves are still relatively strong. Detonation re-initiation in the reactive gas downstream of the inert layer occurs at the gas compressed by the collision of the transverse waves, and thus is referred to as a *cellular-instability-controlled* re-initiation. (2) If an inert layer is sufficiently thick, the detonation wave front has fully decayed to a planar shock when it exits the inert layer, and re-initiation still occurs downstream as a result of planar shock compression only, which is thus referred to as a *planar-shock-induced* re-initiation. Between these two regimes there is a transition region where the wave front is not yet fully planar, and thus perturbations by the transverse waves still play a role in the re-initiation. For the highly unstable case, re-initiation only occurs via the cellular-instability-controlled mechanisms below a critical thickness of the inert layer. Additional simulations considering detailed chemical kinetics demonstrate that the critical re-initiation behaviors of an unstable stoichiometric mixture of hydrogen-air at 1 atm and 295 K are consistent with the finding from the two-step kinetic model for a highly unstable reactive mixture.

Keywords: Detonation re-initiation; inert layer; cellular instabilities; detonation in non-uniform media; gap test for gaseous detonation

1. Introduction

The phenomena of gaseous detonation waves propagating in a spatially non-uniform medium containing pockets of inert or non-detonable gases can be found in numerous real-world scenarios. One such example is in the combustion chamber of an RDE (Rotating Detonation Engine) [1], where separate fuel and oxidizer injection may lead to incomplete mixing, thus, giving rise to regions with low detonability. Another example is in the event of an explosion of accidentally released fuel clouds. Due to the incomplete mixing between the released fuel and ambient air, regions of detonable mixtures are surrounded or separated by non-detonable gases. In order to understand the complex dynamics of a detonation propagating in such environments with spatially non-uniform detonability, the core questions as to whether and how a detonation can transmit across a pocket of inert gases must be addressed. A canonical set-up as illustrated in Fig. 1—an incident gaseous detonation wave propagating across a finite-width (δ_i) gap of inert gases embedded in an otherwise homogeneous detonable mixture—can be used to probe the transmission behaviors of gaseous detonations.

Experimental efforts were made, particularly in the 1980s-90s, to examine the transmission of gaseous detonations across an inert layer [2–6]. However, obtaining a reproducible inert layer with abrupt boundaries is difficult in practice. Concerning the uncertainties in the experimental studies, it is perhaps more convenient to tackle this problem using computational analysis. One-dimensional benchmark scenarios of a detonation wave transmitting over a discontinuity in density and temperature [7] and across an inert gap [8] have previously been studied by the authors. For a planar incident detonation, a critical inert-layer thickness, $\delta_{\mathrm{i,cr}}$, beyond which the incident detonation cannot be re-initiated in the downstream reactive region, can be identified for sufficiently unstable mixtures, i.e., with chemical kinetics characterized by a sufficiently high activation energy [8]. Although this finding is limited to one dimension, it indicates that the temperature sensitivity of the induction and reaction rates influences the critical re-initiation behaviors of a detonation wave being subjected to the perturbation of an inert gap.

In realistic gaseous detonations, temperature-dependent chemical kinetics are coupled with the complex of multi-dimensional hydrodynamics. This coupling manifests itself as a multi-dimensionally unstable detonation structure featuring triple-point interactions between transversely propagating shock waves and a non-planar leading shock front. For a highly unstable mixture characterized by a relatively high global activation energy, e.g., in undiluted fuel-air and fuel-oxygen mixtures, the detonation wave exhibits an irregular cellular structure; for a weakly unstable mixture with a relatively low activation energy, e.g., argon-diluted mixtures, the cellular detonation structure is regular. Previous studies have revealed that highly and weakly unstable detonations behave very differently in various critical phenomena, including transmission into an unconfined space [9] and propagation with lateral expansions or mass divergence [10–12]. A common finding of these studies is that, for highly unstable detonations while subjected to losses or perturbations, the intrinsic cellular instabilities play a more significant role in controlling the propagation and re-initiation capabilities of the detonation wave. The question, thus, arises as to how highly and weakly unstable detonations differently respond to the perturbation of an inert gap. In other words, how does the nature of cellular instabilities affect the capability and mode of re-initiation of a gaseous detonation transmitting across an inert gap?

This present work is a computational effort in seeking an answer to the aforementioned questions. Two-dimensional simulations with simplified two-step kinetic models representing highly and weakly unstable mixtures are performed to (1) examine whether a critical inert-gap thickness for re-initiation exists and (2) elucidate in detail the failure and re-initiation processes downstream from the inert gap in both mixtures. In addition, a set of simulations with detailed chemical kinetics is performed to demonstrate the transmission behaviors across an inert pocket embedded in a stoichiometric mixture of hydrogen and air, which is a typical fuel-oxidizer mixture used in air-breathing pressure-gain combustors [13].

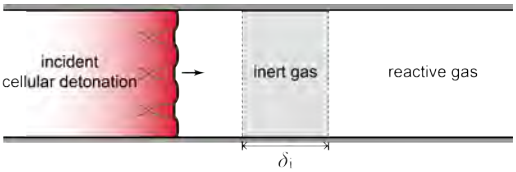

Fig. 1: Schematic illustration showing the problem of an incident cellular detonation wave propagating towards a layer of inert gas with a thickness of δ_i.

2. Model description

The detonation is initiated by a high pressure region with a sinusoidal perturbation and the initiation is sufficiently far upstream such that a fully established cellular CJ (Chapman-Jouguet) detonation is obtained prior to encountering the inert layer of thickness, δ_i in Fig. 1. Diffusive and viscous effects are ignored, such that the system is governed by the two-dimensional reactive Euler equations, i.e.,

$$\frac{\partial \mathbf{U}}{\partial \tilde{t}} + \frac{\partial \mathbf{F}(\mathbf{U})}{\partial \tilde{x}} + \frac{\partial \mathbf{G}(\mathbf{U})}{\partial \tilde{y}} = \mathbf{S}(\mathbf{U}) \qquad (1)$$

with conserved variables $\mathbf{U}$, convective fluxes $\mathbf{F}(\mathbf{U})$

and $\mathbf{G(U)}$, and source terms $\mathbf{S(U)}$ given by,

$$\begin{aligned}
\mathbf{U} &= (\tilde{\rho}, \tilde{\rho}\tilde{u}, \tilde{\rho}\tilde{v}, \tilde{\rho}\tilde{e}, \tilde{\rho}Y_n)^T \\
\mathbf{F(U)} &= (\tilde{\rho}\tilde{u}, \tilde{\rho}\tilde{u}^2 + \tilde{p}, \tilde{\rho}\tilde{u}\tilde{v}, \tilde{u}(\tilde{\rho}\tilde{e} + \tilde{p}), \tilde{\rho}\tilde{u}Y_n)^T \\
\mathbf{G(U)} &= (\tilde{\rho}\tilde{v}, \tilde{\rho}\tilde{u}\tilde{v}, \tilde{\rho}\tilde{v}^2 + \tilde{p}, \tilde{v}(\tilde{\rho}\tilde{e} + \tilde{p}), \tilde{\rho}\tilde{v}Y_n)^T \\
\mathbf{S(U)} &= (0, 0, 0, 0, \tilde{\omega_n})^T.
\end{aligned} \tag{2}$$

Here $\tilde{\rho}$, $\tilde{u}$, $\tilde{v}$, $\tilde{p}$, $\tilde{e}$ are the density, particle velocities in x and y directions, pressure and specific total energy, respectively. The chemical species are represented by subscript n, where Y_n are their mass fractions, and $\tilde{\omega_n}$ their production rates. Two chemical kinetic models were used.

2.1. Two-step chemical kinetic model

As the first step, the heat release was described by a two-step chemical kinetic model. The reaction is split into a thermally neutral induction stage and a reaction stage. Both stages have a temperature-sensitive Arrhenius form of the reaction rate. The system of equations is,

$$\begin{aligned}
\frac{\mathrm{d}(\rho\xi)}{\mathrm{d}t} &= H(1-\xi)\rho k_\mathrm{I} \exp\left[E_\mathrm{I}\left(\frac{1}{T_\mathrm{vN}} - \frac{1}{T}\right)\right], \\
\frac{\mathrm{d}(\rho\lambda)}{\mathrm{d}t} &= (1 - H(1-\xi))\rho k_\mathrm{R}(1-\lambda)\exp\left(\frac{-E_\mathrm{R}}{T}\right)
\end{aligned} \tag{3}$$

with the step function,

$$H(1-\xi) = \begin{cases} 1 & \xi < 1 \\ 0 & \xi \geq 1. \end{cases} \tag{4}$$

Here ξ is progress variable, so that at the end of the induction process all of the fuel is converted to radicals instantaneously. Then λ can be thought of as the mass fraction of product. The parameters k_I and k_R are rate constants, and E_I and E_R are activation energies for the induction and reaction steps, respectively.

In the above equations, the activation energies have been non-dimensionalized by RT_0, where R and T_0 are the gas constant and the temperature of the unburnt gas, respectively. However, an alternate non-dimensionalization which is commonly used in the literature (see for example [14]) has been introduced. The modified activation energies, ϵ_I and ϵ_R, are non-dimensionalized by RT_vn, where T_vn is the von Neumann shock temperature. The activation energy of the induction process, ϵ_I was either 7 or 9. The smaller value of $\epsilon_\mathrm{I} = 7$ corresponds to a weakly unstable wave, whereas the larger value of $\epsilon_\mathrm{I} = 9$ corresponds to a highly unstable wave. In one-dimension, the stability limit is at $\epsilon_\mathrm{I} = 9$. It should also be noted that further increase and decrease in the activation energy has been performed and does not change the qualitative behaviors reported in this paper. Therefore, the present results encompass the full range of behavior.

The induction length of the corresponding steady ZND detonation, Δ_I, is set to unity. The chemical kinetic model, non-dimensionalization of state and flow variables, and the scaling of rate constants are detailed in [15]. For simplicity, the initial temperature and pressure were prescribed to be constant throughout the domain. Thus, from the reactive to inert gas there is a change in the energetics only.

The simulation was based upon a uniform Cartesian grid, and the Strang splitting method was adopted to treat separately the hydrodynamic process and the reactive process. The MUSCL-Hancock scheme with the van Leer non-smooth slope limiter and a Harten-Lax-van Leer-contact (HLLC) approximate solver was used [16]. To optimize the simulation efficiency, the entire flow solver [17–19] was implemented by the parallel computing platform Compute Unified Device Architecture (CUDA), enabled by Nvidia Tesla V100 graphics processing units (GPU). The resolution was 10 grid points per Δ_I, but a resolution test was performed at 20 grid points per Δ_I. Some results from the resolution test are given in the supplementary material. The domain width, W, was 300 Δ_I. A periodic boundary condition was applied to the top and bottom of the domain, and the left boundary was transmissive. Numerical soot foils were generated by tracking the maximum pressure in the domain.

2.2. Detailed chemical kinetic model

A more detailed chemical kinetic model was also used. The kinetic mechanism is a hydrogen-air kinetic mechanism developed by Westbrook [20], where nitrogen is treated as a dilutent. There are 17 elementary reactions and 9 species, including H_2, O_2, H, O, OH, H_2O, HO_2, H_2O_2 and N_2. The reactive mixture was stoichiometric hydrogen-air, i.e., $2H_2 + O_2 + 3.76N_2$, and the inert gas was air, i.e., $O_2 + 3.76N_2$. The gases were both initially at ambient pressure and temperature, i.e., 1 atm and 295 K. In this case since there is a difference in mixture molecular weight between the reactive and inert gases, there is a corresponding difference in density under the constant ambient pressure and temperature constraint. That is, there is a change in density across the boundaries of the inert layer, with the layer being more dense than the surrounding reactive gas.

The simulation employs the AMROC framework (adaptive mesh refinement in object-oriented C++), detailed in [21–23]. The domain width was 30 mm, which corresponds to about 150 ZND induction lengths, 150 Δ_I. The coarsest grid was 8 cells per mm, and three additional levels of refinement were allowed, with refinement factors of 2, 4 and 4, respectively. The resolution at the highest level was therefore ($8 \times 2 \times 4 \times 4$ =) 256 cells per mm, or $\Delta x = 3.9$ µm. A resolution test was also performed at double the base resolution, i.e. 16 cells per mm. Some results from the resolution test are given in the supplementary material. The top and bottom boundaries of the domain were reflective, and the

left boundary was transmissive. Numerical soot foils were generated by tracking the maximum vorticity in the domain.

3. Results and discussion

3.1. Transmission into inert medium; analysis of the transmitted wave

In this section, results with the two-step chemical kinetic mechanism are presented. First, consider the transmission of the detonation wave from the reactive to inert gas only. This will describe the transmitted wave at the exit of the inert layer for any given inert thickness, $\delta_{\rm i}$. The process is shown in Fig. 2 via numerical soot foils, where Figs. 2**(a)** and **(b)** are for the highly unstable $\epsilon_{\rm I} = 9$ and weakly unstable $\epsilon_{\rm I} = 7$ cases respectively. The vertical dashed line indicates the boundary between the reactive and inert gas which is at $x = 0$. The intrinsic cellular structure of the incident detonation is more regular for the weakly unstable, lower activation energy case, i.e. $\epsilon_{\rm I} = 7$ in Fig. 2**(b)**. By contrast, the incident detonation structure is irregular for the highly unstable case, i.e. $\epsilon_{\rm I} = 9$ in Fig. 2**(a)**. When the detonation enters the inert layer, there is a reduction in the energy release from chemical reactions. The detonation decays; the strength of the shock front decreases overall, including the transverse waves, thus the pressure behind the detonation decreases. Eventually, a transmitted shock wave with constant velocity is obtained.

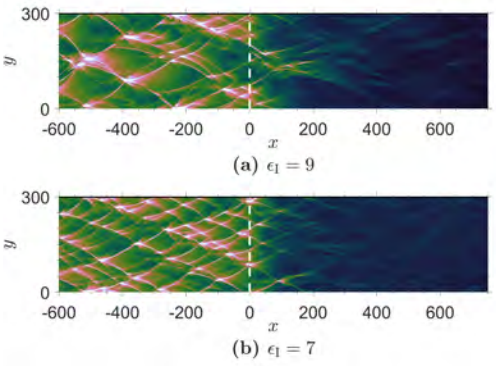

(a) $\epsilon_{\rm I} = 9$

(b) $\epsilon_{\rm I} = 7$

Fig. 2: Numerical soot foils for the detonation transmission from reactive to inert gas for the **(a)** highly unstable, $\epsilon_{\rm I} = 9$, and **(b)** weakly unstable, $\epsilon_{\rm I} = 7$ cases. The vertical dashed line at $x = 0$ indicates the initial boundary between the reactive and inert gases.

The goal is to represent quantitatively the transient decay process. To begin, this two-dimensional pressure field was reduced to an average one-dimensional pressure field by averaging across the vertical y-axis as follows,

$$\bar{p} = \frac{\int p\, dy}{W}. \tag{5}$$

The average shock location, $x_{\rm shock}$, was defined to be where $\bar{p}$ becomes greater than some threshold pressure, and its location was calculated by interpolation. When repeated throughout the decay, $x_{\rm shock}$ was obtained as a function of time, and the average shock speed $M_{\rm shock}$ can be calculated. Finally, the average shock pressure $p_{\rm shock}$ was found from $M_{\rm shock}$ with the Rankine-Hugoniot relations.

Also of interest is the distribution of pressure near the shock front. Consider the region around $x_{\rm shock}$, which extends 25 induction lengths, 25 $\Delta_{\rm I}$ in front of $x_{\rm shock}$, and 25 $\Delta_{\rm I}$ behind $x_{\rm shock}$. The pressure at each computational cell within the region was recorded, and used to calculate a PDF (probability density function) of pressure. When repeated throughout the decay, the PDF shows how the pressure distribution near the shock changes. Finally, the pressure analysis was repeated for five runs, and an ensemble average was taken. that from run to run the location of the inert layer was varied, so that the structure of the incident detonation changes. The results are shown in Fig. 3. The x-axis is the shock location $x_{\rm shock}$, and the y-axis is the pressure. Again, the vertical dashed line indicates the reactive-inert boundary at $x = 0$. The solid black line is the average shock pressure, $p_{\rm shock}$. For the incident detonation, $p_{\rm shock}$ fluctuates around $p_{\rm vn}$, the von Neumann shock pressure which is shown by a horizontal dashed line. After the detonation enters the inert gas, $p_{\rm shock}$ decreases. Eventually, the final shock with pressure, $p_{\rm f}$ in Fig. 3 will be obtained. The coloured contour shows the PDF of pressure near the shock front, where the color indicates the recurrence of that pressure value, or the probability that the pressure is the indicated value. For example, for the incident detonation the pressure near the front ranges from $p < 20$ to $p > 80$, and there are many points with $p \approx p_{\rm vn}$ and very few points with $p = 80$. After the detonation enters the inert gas, the pressure range narrows, and in particular the maximum pressure obtained near the front decreases.

Large pressure fluctuations above $p_{\rm vn}$ remain until about $x_{\rm shock} = 150$–200, which corresponds roughly to the disappearance of the cellular structure in the soot foils of Fig. 2. Therefore, after this point there has been significant damping of the transverse waves. The smaller pressure fluctuations above $p_{\rm f}$ die off by about $x_{\rm shock} = 500$–600. After this point, $p_{\rm shock} \approx p_{\rm f}$ and the transmitted wave is no longer changing.

3.2. Transmission across inert layer; detonation re-initiation

3.2.1. Two-step chemistry; highly unstable mixture

Now consider a layer of inert gas with finite thickness, $\delta_{\rm i}$. Typical numerical soot foils for the highly unstable case, i.e. $\epsilon_{\rm I} = 9$ are shown in Fig. 4, where the inert layer thicknesses are $\delta_{\rm i} = 100$, 150, 200, and 500, respectively. The vertical dashed lines show the two boundaries of the inert layer. When $\delta_{\rm i} \leq 150$, the

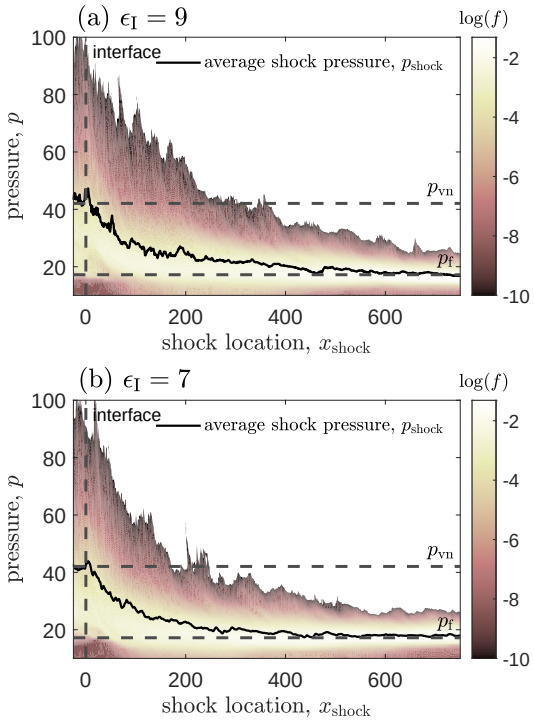

Fig. 3: The average shock pressure, $p_{\rm shock}$ and the PDF (probability density function) of pressure plotted against the shock location, $x_{\rm shock}$ for the **(a)** highly unstable, $\epsilon_{\rm I} = 9$, and **(b)** weakly unstable, $\epsilon_{\rm I} = 7$ cases. The vertical dashed line at $x = 0$ indicates the initial boundary between the reactive and inert gases; the horizontal dashed lines are the von Neumann shock pressure, $p_{\rm vn}$ and the final shock pressure, $p_{\rm f}$.

detonation is successfully transmitted downstream of the inert layer. On the other hand, when $\delta_{\rm i} \geq 200$, the detonation cannot be re-initiated downstream. Therefore, the critical thickness, $\delta_{\rm i,cr}$ is 175 ± 25.

The re-initiation occurs at the collision of the transverse waves in the reactive gas downstream of the inert layer. The gas which is compressed by the collision of the transverse waves reacts more rapidly, and this rapid release of energy strengthens the subsequent Mach stem. Therefore, the re-initiation mechanism is referred to as the *cellular-instability-controlled* mechanism. This type of re-initiation is consistent with Figs. 2**(a)** and 3**(a)**, in that the detonation cellular structure, i.e. some stronger transverse waves or large fluctuations on the PDF survive up to about $x_{\rm shock} = 200$. Thus, for these inert thicknesses of $\delta_{\rm i} < 200$ the transmitted wave at the exit of the inert layer is still significantly cellular.

A re-initiation distance, $l_{\rm r}$, was defined to be the distance between the downstream boundary (i.e. exit) of the inert layer and the point where the average shock pressure $p_{\rm shock}$ becomes $\geq p_{\rm vn}$. The results are plotted in Fig. 5 for the five runs. The re-initiation distance, $l_{\rm r}$ increases as the inert thickness, $\delta_{\rm i}$ increases up until failure. However, there is some variation from run to run in the $l_{\rm r}$ measured at each $\delta_{\rm i}$. This is likely due to the irregularity of the cellular structure of the incident detonation. The critical thickness, $\delta_{\rm i,cr}$ also varied between runs, ranging from 125–225 as shown by the vertical dashed lines and shaded region.

3.2.2. Two-step chemistry, weakly unstable mixture

Now consider the weakly unstable mixture, i.e. $\epsilon_{\rm I} = 7$. Typical numerical soot foils are shown in Fig. 6, where the inert layer thickness ranges from $\delta_{\rm i} = 50$–600. In this case there is no critical thickness, i.e., the detonation is always re-initiated downstream. In a similar way, in Fig. 7 the re-initiation length, $l_{\rm r}$ is plotted for the five runs.

When $\delta_{\rm i} \lesssim 150$, some strong transverse waves are still present on the transmitted wave when the wave exits the inert layer, as was seen on the soot foil of Fig. 2**(b)** and by the large fluctuations on the PDF of Fig. 3**(b)**. Thus, the re-initiation mechanism is similar to that for the highly unstable, $\epsilon_{\rm I} = 9$ case from before. The cellular-instability-controlled type of re-initiation occurs at the collision of transverse waves. In addition, the re-initiation length, $l_{\rm r}$ increases with increased inert thickness, $\delta_{\rm i}$ as before.

On the other hand, when $\delta_{\rm i} \geq 500$, the transmitted wave at the exit of the inert layer is no longer changing as was seen on the PDF of Fig. 3**(b)**. The majority of the pressure fluctuations have died out and the wave front is essentially a planar shock with shock pressure $p_{\rm f}$. Therefore, the re-initiation downstream is induced by compression of a planar shock wave, and thus, referred to as the *planar-shock-induced* mechanism. As can be seen on the last two soot foils in Figs. 6**(g)** and **(h)** for $\delta_{\rm i} = 500$ and 600, the re-initiation occurs uniformly across the channel width. Excerpts of the flow field showing further details of this re-initiation process are given in the supplementary material. In addition, the re-initiation length, $l_{\rm r}$ in Fig. 7 does not change. In fact, $l_{\rm r}$ plateaus to a constant value which is equal to that for one-dimensional planar shock initiation with shock pressure $p_{\rm f}$. This limit is shown by the horizontal line in Fig. 7.

Between these two regimes, i.e. for $200 < \delta_{\rm i} < 400$, there is a transition region where the transmitted shock is not yet fully planar. The transverse waves are weakened but still contribute to the ignition in the downstream gas. Thus, the re-initiation on the soot foils of Fig. 6 is still somewhat spotty. In addition, the shock pressure $p_{\rm shock}$ is still greater than $p_{\rm f}$. Therefore, the re-initiation length is shorter than that for the planar shock with shock pressure $p_{\rm f}$ (the limit in Fig. 7 shown by the horizontal line).

Note that there is less variation from run to run in the re-initiation lengths as compared to the highly unstable, $\epsilon_{\rm I} = 9$ case from before. For comparison, the standard deviation of the re-initiation length, $\sigma_{l_{\rm r}}$ is plotted against the inert thickness, $\delta_{\rm i}$ in Fig. 8 for both cases. Where the cellular-instability-controlled type

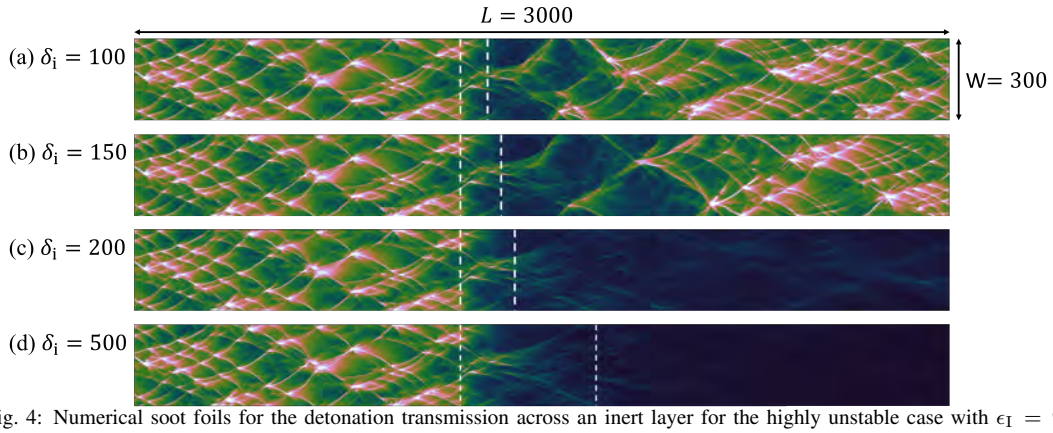

Fig. 4: Numerical soot foils for the detonation transmission across an inert layer for the highly unstable case with $\epsilon_I = 9$, and inert thicknesses **(a)** $\delta_i = 100$, **(b)** 150, **(c)** 200, and **(d)** 500. The vertical dashed lines indicate the initial upstream and downstream boundaries of the inert layer.

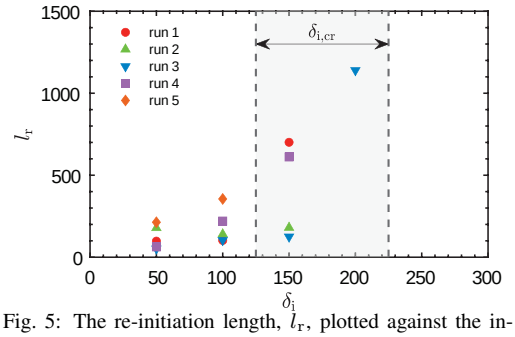

Fig. 5: The re-initiation length, l_r, plotted against the inert thickness, δ_i, for the highly unstable $\epsilon_I = 9$ case. The vertical dashed lines and a shaded region show the range of values measured for the critical thickness, $\delta_{i,cr}$.

of re-initiation exists, i.e. for $\delta_i \leq \sim 150$, the standard deviation is always higher for the highly unstable $\epsilon_I = 9$ case than that for the weakly unstable $\epsilon_I = 7$ case. This is because the incident detonation cellular structure is more irregular. In addition, for $\epsilon_I = 7$ the standard deviation starts to decrease afterward as the inert thickness increases. This is because the re-initiation mechanism transitions from the cellular-instability-controlled type of re-initiation, where the cyclic nature of the cellular structure plays a key role, to the one-dimensional planar-shock-induced type of re-initiation.

Finally, note that this absence of a critical thickness is unrealistic. This seemingly illogical result could be explained by two factors. In general, a detonation wave is followed by an expansion wave called the Taylor wave which further expands the detonation products. Then, given an infinitely long inert layer, the final transmitted shock would not be constant at p_f, but this shock would further decay to an acoustic wave. Therefore, failure would occur for some inert thickness that gives a transmitted shock with shock pressure lower than p_f. In addition, in general there will be energy and momentum losses that are not accounted for in the present study. Such losses would hamper the re-initiation, particularly as the length scales, i.e. the inert thickness and re-initiation length increase. Nevertheless, detecting this limit is not the goal of the present study.

3.2.3. Detailed chemistry

Finally, consider the simulations with the detailed kinetic mechanism for hydrogen-air. Figure 9 shows the numerical soot foils for inert thicknesses $\delta_i = 0.06$ cm and 0.08 cm. The detonation is successfully re-initiated when $\delta_i = 0.06$ cm, but fails to re-initiate when $\delta_i = 0.08$ cm. Therefore, the critical thickness, $\delta_{i,cr} = 0.07 \pm 0.01$ cm. The re-initiation mechanism can again be classified as the cellular-instability-controlled type of re-initiation, with detonation onset for $\delta_i = 0.06$ occurring at the collision of the transverse waves near the top of the domain. Thus, the result is qualitatively similar to that for the highly unstable detonation. This is compatible with experimental evidence that suggests that such undiluted hydrogen-air detonations are relatively unstable [24, 25].

4. Concluding remarks

In this study, the dynamics of the perturbation of cellular detonations by a layer of inert gas is explored via two-dimensional computational simulations. In particular, the role of the cellular instabilities and modes of re-initiation of a gaseous detonation transmitting across an inert gap are demonstrated. Two types of mixtures are considered, namely, a highly unstable and a weakly unstable mixture in which highly irregular and regular cellular detonations occur, respectively.

For the highly unstable reactive mixture, results from the present study clarified the role of the transverse wave instabilities in both the existence of a

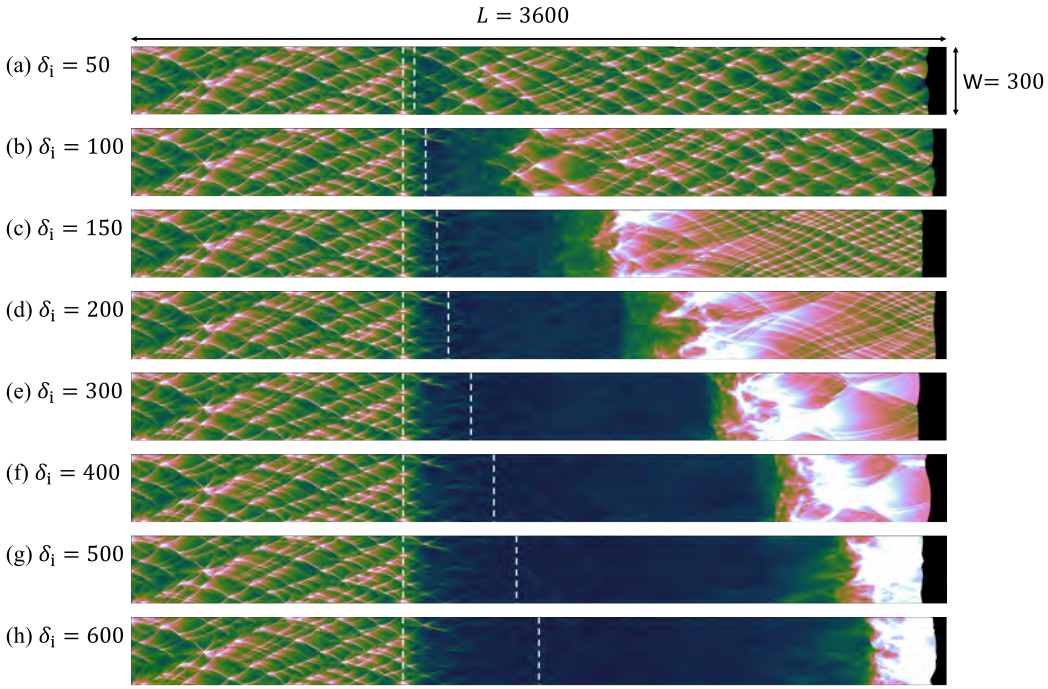

Fig. 6: Numerical soot foils for the detonation transmission across an inert layer, for the weakly unstable case with $\epsilon_I = 7$, and inert thicknesses **(a)** $\delta_i = 50$, **(b)** 100, **(c)** 150, **(d)** 200, **(e)** 300, **(f)** 400, **(g)** 500, and **(h)** 600. The vertical dashed lines indicate the initial upstream and downstream boundaries of the inert layer.

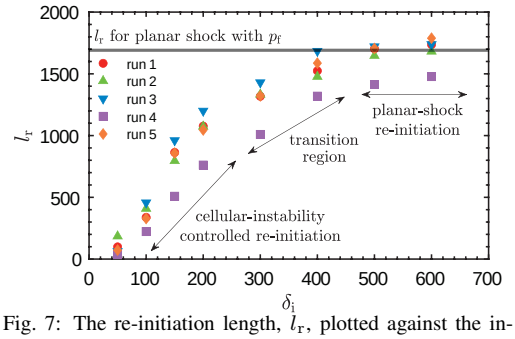

Fig. 7: The re-initiation length, l_r, plotted against the inert thickness, δ_i, for the weakly unstable $\epsilon_I = 7$ case. The horizontal line shows the re-initiation length for a one-dimensional planar shock with shock pressure, p_f. The regions of the cellular-instability-controlled type and the planar-shock-induced type of re-initiation are labelled, along with a transition region between the two.

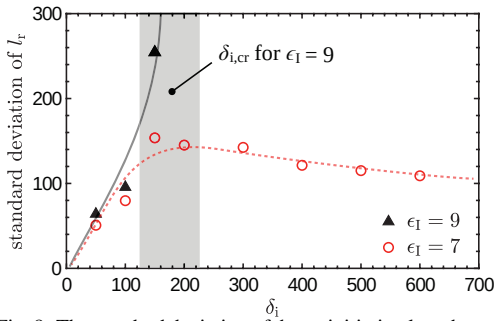

Fig. 8: The standard deviation of the re-initiation length, σ_{l_r}, plotted against the inert thickness, δ_i for the highly unstable, $\epsilon_I = 9$ and weakly unstable, $\epsilon_I = 7$ cases. The shaded region shows the range for the critical thickness, $\delta_{i,cr}$ for the highly unstable, $\epsilon_I = 9$ case.

critical inert-gap thickness and the downstream re-initiation, at which the detonation onset occurs at the gas compressed by the collision of the transverse waves. This re-initiation mechanism was called the cellular-instability-controlled type of re-initiation. In addition, the detonation fails to re-initiate if the transverse waves are not sufficiently strong, and therefore if the inert layer is too thick. Thus, a critical inert thickness can be defined. These salient observations captured by the results using the simplified two-step model agree closely with those using the detailed chemical kinetic model for a realistic unstable stoichiometric mixture of hydrogen-air.

Another important finding is that for the weakly unstable reactive mixture, the detonation is always re-initiated downstream of the inert layer, i.e. no critical thickness exists, and a second mode of re-initiation occurs. When the inert layer is thin, the re-initiation is of the cellular-instability-controlled type where transverse waves are still relatively strong and dominate

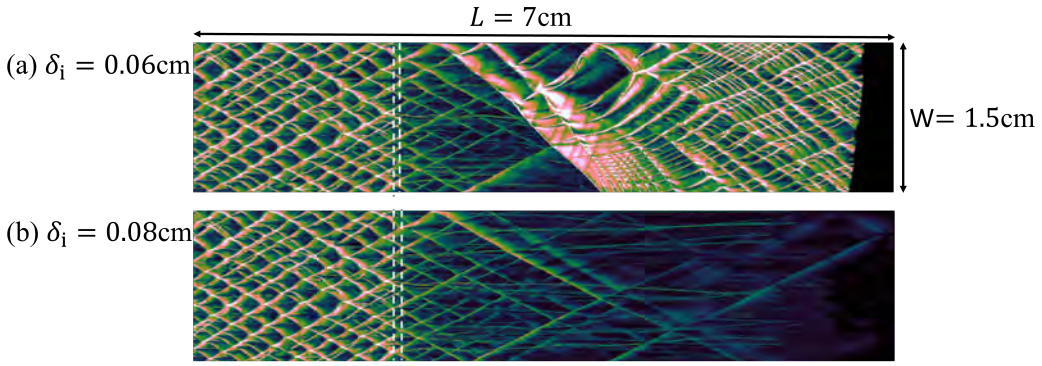

Fig. 9: Numerical soot foils for the detonation transmission across an inert layer, for the detailed chemical kinetic model with stoichiometric hydrogen-air at 1 atm and 295 K, and inert thicknesses **(a)** $\delta_i = 0.06$ cm, and **(b)** 0.08 cm. The vertical dashed lines indicate the initial upstream and downstream boundaries of the inert layer.

the re-initiation process. As the inert layer becomes thicker, the transverse waves are weaker when the wave exits the layer, and the wave transmitted into the downstream reactive gas becomes more and more planar. The re-initiation mechanism transitions to that of planar-shock ignition, and is therefore called a planar-shock-induced re-initiation. Therefore, weakly unstable mixtures are found to be less reliant on the transverse wave instabilities of the detonation cellular structure for re-initiation. This result of the non-existence of a critical thickness for sufficiently stable mixtures is consistent with the authors' previous one-dimensional simulations [8]. It was postulated that in order to define a critical thickness, the purely one-dimensional far field decay of the transmitted shock could be considered.

This study thus shows conclusively that the critical thickness is mainly the result of the residual effects of the intrinsic cellular instabilities of the incident detonation on the downstream reactive mixture. Altogether, the present results are consistent with those for other critical phenomena [10–12, 26, 27], where in general detonation propagation and re-initiation for more stable mixtures are more closely approximated by a one-dimensional model, and for highly unstable mixtures the intrinsic cellular instabilities play a more significant role.

Acknowledgments

Kelsey Tang-Yuk was supported by the Fonds de recherche du Québec - Nature et technologies, file number 270439.

References

[1] F. Lu, E. Braun, Rotating detonation wave propulsion: Experimental challenges, modeling, and engine concepts, J. Propul. Power 30 (2014) 1125–1142.

[2] D. Bull, J. Elsworth, M. McLeod, D. Huges, Initiation of unconfined gas detonations in hydrocarbon-air mixtures by a sympathetic mechanism, Gasdynamics of Detonations and Explosions 75 (1979) 61–72.

[3] T. Gavrilenko, A. Krasnov, Y. A. Nikolaev, Transfer of a gas detonation through an inert gas "plug", Combust. Explo. Shock 18 (2) (1982) 240–244.

[4] D. Bjerketvedt, O. Sonju, I. Moen, The influence of experimental condition on the reinitiation of detonation across an inert region, Progr. Astronaut. Aero. 106 (1986) 109–130.

[5] T. Engebretsen, D. Bjerketvedt, O. Soenju, Propagation of gaseous detonations through regions of low reactivity, Progr. Astronaut. Aero. 153 (1993) 324–324.

[6] A. Teodorczyk, F. Benoan, Interaction of detonation with inert gas zone, Shock Waves 6 (4) (1996) 211–223.

[7] K. Tang-Yuk, X. Mi, J. Lee, H. Ng, Transmission of a detonation across a density interface, Shock Waves 28 (2018) 967–979.

[8] K. C. Tang-Yuk, X. C. Mi, J. H. S. Lee, H. D. Ng, R. Deiterding, Transmission of a detonation wave across an inert layer, Combust. Flame 236 (2022) 111769.

[9] J. Lee, On the critical tube diameter, in: J. Bowen (Ed.), Dynamics of Exothermicity, Gordon and Breach, Amsterdam, 1996, p. 321.

[10] M. Radulescu, J. Lee, The failure mechanism of gaseous detonations: experiments in porous wall tubes, Combust. Flame 131 (2002) 29–46.

[11] Q. Xiao, M. Radulescu, Role of instability on the limits of laterally strained detonation waves, Combust. Flame 220 (2020) 410–428.

[12] Q. Xiao, M. Radulescu, Dynamics of hydrogen–oxygen–argon cellular detonations with a constant mean lateral strain rate, Combust. Flame 215 (2020) 437–457.

[13] V. Anand, A. St. George, R. Driscoll, E. Gutmark, Investigation of rotating detonation combustor operation with H_2-air mixtures, Int. J. Hydrogen Energy 41 (2) (2016) 1281–1292.

[14] E. Schultz, J. Shepherd, Validation of Detailed Reaction Mechanisms for Detonation Simulation, Tech. rep., California Institute of Technology, Graduate Aeronautical Laboratories, Pasadena (2000).

[15] H. Ng, M. Radulescu, A. Higgins, N. Nikiforakis, J. Lee, Numerical investigation of the instability for one-dimensional Chapman-Jouguet detonations with chain-branching kinetics, Combust. Theor. Model 9

(2005) 385–401.
[16] E. Toro, Riemann Solvers and Numerical Methods for Fluid Dynamics, Springer-Verlag, Berlin, 1997.
[17] C. Kiyanda, G. Morgan, N. Nikiforakis, H. Ng, High resolution GPU-based flow simulation of the gaseous methane-oxygen detonation structure, J. Visual-Japan 18 (2) (2015) 273–276.
[18] X. Mi, A. Higgins, H. Ng, C. Kiyanda, N. Nikiforakis, Propagation of gaseous detonation waves in a spatially inhomogeneous reactive medium, Phys. Rev. Fluids 2 (5) (2017) 053201.
[19] X. Mi, A. Higgins, C. Kiyanda, H. Ng, N. Nikiforakis, Effect of spatial inhomogeneities on detonation propagation with yielding confinement, Shock Waves 28 (5) (2018) 993–1009.
[20] C. Westbrook, Chemical kinetics of hydrocarbon oxidation in gaseous detonations, Combust. Flame 46 (1982) 191–210.
[21] R. Deiterding, available at <http://amroc.sourceforge.net>.
[22] R. Deiterding, Parallel adaptive simulation of multidimensional detonation structures, Ph.D. thesis, Brandenburgischen Technischen Universität, Cottbus, Germany (2003).
[23] R. Deiterding, A parallel adaptive method for simulating shock-induced combustion with detailed chemical kinetics in complex domains, Comput. Struct. 87 (11-12) (2009) 769–783.
[24] C. Guirao, R. Knystautas, J. Lee, A summary of hydrogen-air detonation experiments, Tech. Rep. SAND-87-7128, Sandia National Laboratories, Albuquerque, NM, USA (1989).
[25] B. Taylor, D. Kessler, V. Gamezo, E. Oran, Numerical simulations of hydrogen detonations with detailed chemical kinetics, Proc. Combust. Inst. 34 (2) (2013) 2009–2016.
[26] N. Mehrjoo, Y. Gao, C. B. Kiyanda, H. D. Ng, J. H. Lee, Effects of porous walled tubes on detonation transmission into unconfined space, Proc. Combust. Inst. 35 (2) (2015) 1981–1987.
[27] H. Xu, X. Mi, C. B. Kiyanda, H. D. Ng, J. H. Lee, C. Yao, The role of cellular instability on the critical tube diameter problem for unstable gaseous detonations, Proc. Combust, Inst. 37 (3) (2019) 3545–3553.